ICANS-VI

INTERNATIONAL COLLABORATION ON ADVANCED NEUTRON SOURCES

June 27 - July 2, 1982

SOME ASPECTS OF THE NEUTRONICS OF THE SIN NEUTRON SOURCE

F. Atchison and W.E. Fischer
Schweizerisches Institut für Nuklearforschung
CH-5234 Villigen, Switzerland

and

B. Sigg
Institut für Reaktortechnik, ETHZ
CH-5303 Würenlingen, Switzerland

ABSTRACT

Some results from both experiment and calculation, obtained as part of the optimisation study for the SIN neutron source are presented.

SOME ASPECTS OF THE NEUTRONICS OF THE SIN NEUTRON SOURCE

F. Atchison and W.E. Fischer
Schweizerisches Institut für Nuklearforschung
CH-5234 Villigen, Switzerland

and

B. Sigg
Institut für Reaktortechnik, ETHZ
CH-5303 Würenlingen, Switzerland

1. INTRODUCTION

The current state of the SIN neutron source project is described elsewhere in these proceedings [1]. In this report we present some results, from both experiment and calculation, obtained as part of our detailed design study.

The overall source optimization is a several-year program and has, as its (usual) goal, the production of the best neutron source with the available resources. The major areas of study are:

(i) The neutronic optimization of the source: reconciliation of conflicting neutronic requirements of beam guides and thermal tubes, production of adequately low backgrounds, etc.

(ii) The thermofluid dynamics of the target.

(iii) The practical aspects of producing an operable source: radiological safety, choice of satisfactory materials, etc.

Calculations using both computer codes and "hand built" physics are presented; a brief résumé of the principal computer codes presently available to our project is given in Table I.

2. THE PRODUCTION TARGET

The target material is an eutectic mixture, 55 % Bi, 45 % Pb, of density 10 g/cc. A vertical cylinder of diameter between 10 and 30 cm and of length in excess of 1 m is envisaged, with natural convection in the liquid metal to provide the primary heat transfer mechanism. A major part of our study will be the reconciliation of neutronic and thermofluid-dynamic requirements, to obtain an optimum set of dimensions. The thermofluid dynamics of the

Table I

The principle computer codes available

CODE	COMPUTER	BRIEF DESCIPTION	AREAS OF APPLICATION
HET [1]	VAX-11	Analogue Monte- arlo nucleon-meson transport code.	- Primary production for fast neutrons in target - Energy deposition by the high-energy cascade - Nuclide production by HE spallation reactions - High energy backgrounds for the source
05RSIN	VAX-11	Monte-carlo neutron transport code An extensively modified version of 05R [2]	- Sub-15 Mev neutron effects in the target - Neutronics of the moderator including thermalisation.
EGS [3]	VAX-11	Monte-carlo electromagnetic cascade code.	- Gamma transport throughout the neutron source
DOT-3 [4]	CYBER 170 SERIES	Discrete ordinates neutron transport code	- Shield design
RSYST [5]	CYBER 170 SERIES	One-dimensional transport (Sn) and two-dimensional diffusion code.	- Moderator optimisation studies
ORIHET	VAX-11	Isotope production and decay. A modified version of ORIGEN [6]	- Activation studies throughout the neutron source.

References for Table 1

[1] W.A. COLEMAN & T.W. ARMSTRONG ORNL-4606 (1970)
[2] R.R. COVEYOU et. al. ORNL-3622 (1965)
[3] R.L. FORD & W.R. NELSON SLAC-210 (1978)
[4] W.A. RHOADES & F.R. MYNATT ORNL-TM-4280 (1973)
[5] R. RUEHLE IKE-Ber. 4-12 (1973)
[6] M.J. BELL ORNL-4628 (1973)

HET & 05R are part of the RSIC computer code collection number CCC-178 and ORIGEN is CCC-217.

target are discussed in a separate report in these proceedings (Takeda [2]).

2.1 Neutronic performance

The general neutronic performance, as the target radius is varied, has been calculated using HET. The results are summarized in Fig. 1. The calculation was made using a 530 MeV proton beam in a 2 cm variance Gaussian truncated to 10 cm diameter. As should be expected, fast neutron production increases only slowly once the target radius exceeds that of the beam; similarly for the component of the power dissipation from the high energy cascade.

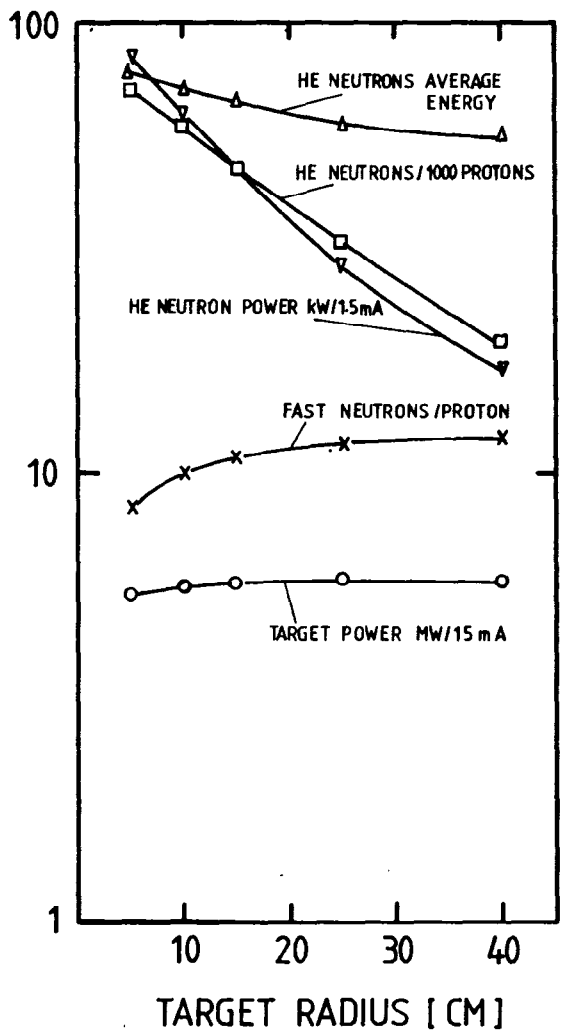

Fig. 1
Variation, with target radius, of target power, fast neutron production and HE neutron production rate, average power and escape power. Calculation for a Pb/Bi target using HET.

A major consideration in the design of the source is the background in thermal beam tubes. The shielding effect of the Pb/Bi is shown by the decrease of both the flux and average energy for the high energy neutron escapes.

2.2 Power dissipation

This is estimated to be approximately 73 % of the incident proton beam power from all sources, with the main contribution coming from ionization loss. The cooling system will have to remove somewhat under 1 MW. A further 17 % of the beam power is used to liberate the neutrons from the target nuclei. The remaining 10 % is deposited in the rest of the source (mainly in the moderator).

2.3 Target activation

The contribution from the residual nuclei of spallation reactions has been calculated using ORIHET. The build-up of activity as a fraction of continuous irradiation time at 1.5 mA, and the decay of activation after a 1 year irradiation are shown in Fig. 2. The target activation should be somewhat less than 1 MCi during normal operation. The power dissipation from these decays is 3 kW, including a 2.6 kW contribution from decay gammas.

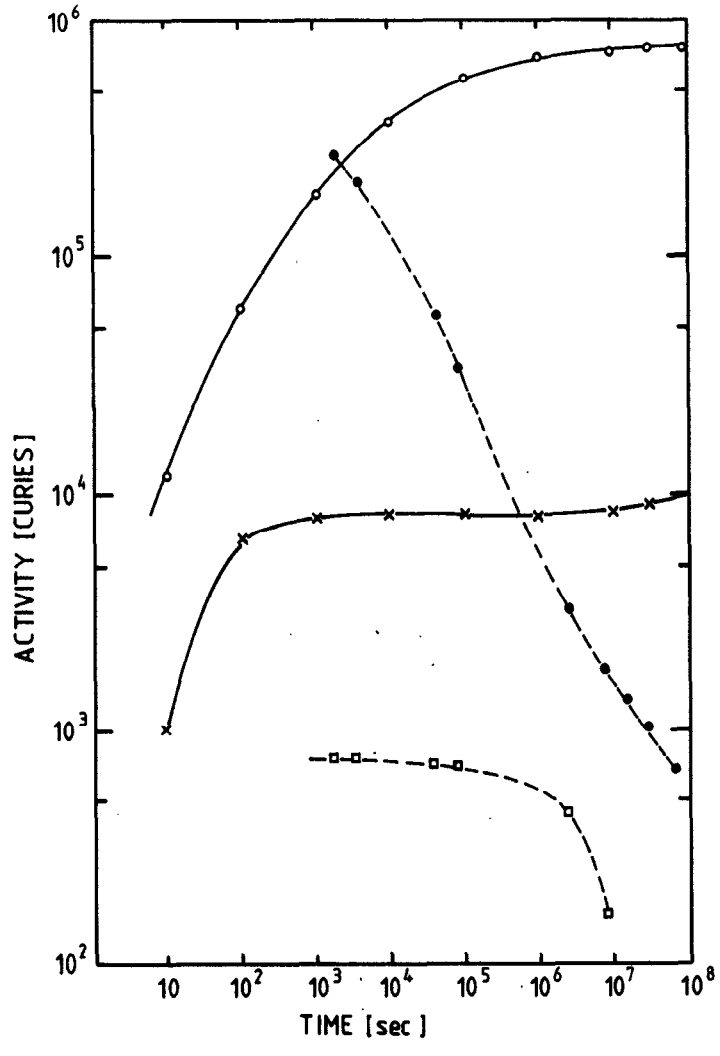

Fig. 2
Build-up and decay of activation for a Pb/Bi target at 1.5 mA and 530 MeV protons. (i) Buildup of total activity (-o-o-o-o-); (ii) Buildup of α-activity (-x-x-x-x-); (iii) Decay of total activity (-•-•-•-•-); (iv) Decay of α-activity (-□-□-□-□-). Decay curves are for time periods following 1 year irradiation.

For the fast and thermal neutrons, the principal product is Po-210; this is estimated to have an equilibrium activity of about 13 kCi, and corresponds to approximately 3 g weight.

2.4 Escape particles

HETC calculations for a 10 cm radius target give an escape evaporation-neutron intensity of 10.4/proton, with an average energy of 1.7 MeV. The calculated distribution of surface brightness is shown in Fig. 3 together with the measured values from ref. [3].

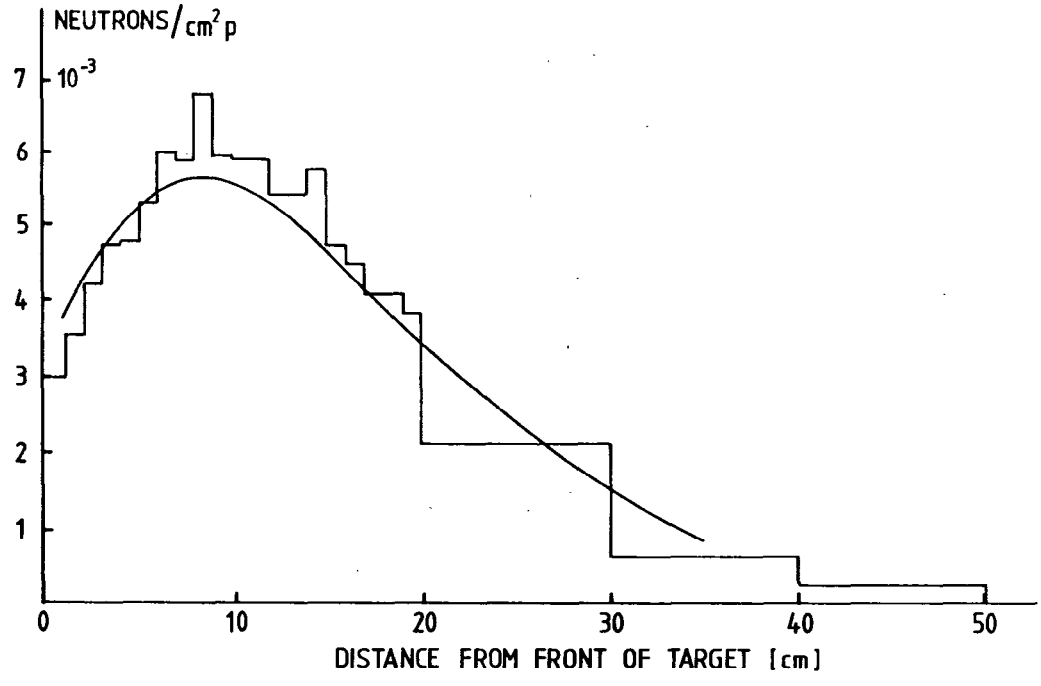

Fig. 3
Surface brightness for fast neutron escapes from a 10 cm radius Pb/Bi target. Histogram - calculation: Solid line - experiment [3].

The high energy particle escapes per incident proton calculated, are:

Neutrons	0.59	of mean energy	71 MeV
Protons	0.008	of mean energy	100 MeV
PI+	0.002	of mean energy	54 MeV
PI-	0.0006	of mean energy	46 MeV

2.5 Gamma Fluxes

A calculation for a 5 cm radius Pb target has been made using the EGS code. The source terms are as follows:

1. Prompt nuclear gammas: 1.2 per incident proton on the basis of the residual excitation being dissipated by emission of a single gamma. The source energy distribution is shown in Fig. 4. The source strength at 1.5 mA proton current is $1.2 \cdot 10^{16}$ photons/sec and 8 kW.

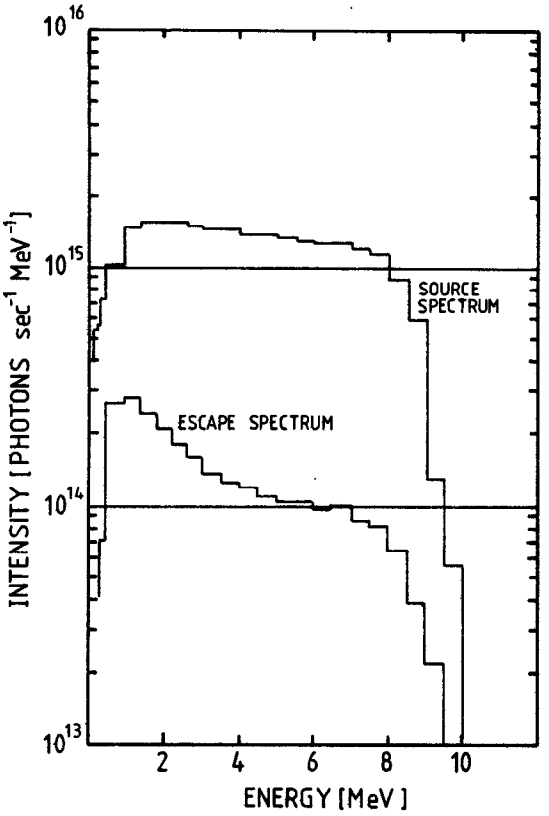

Fig. 4
Integrated source and surface-escape spectra for prompt nuclear gammas

2. π^o decay: 0.024 are produced in the target per incident proton with an energy spectrum approximated by:

$$P(E_{\pi o})dE_{\pi o} = 0.0025\ E_{\pi o} EXP[-(0.05\ E_{\pi o})]dE_{\pi o}$$

Isotropic decay in the CMS system at the production point is used to generate the source gammas. The gamma spectrum is shown in Fig. 5. The source strength at 1.5 mA is $4.5 \cdot 10^{14}$ photons/sec and 6.3 kW.

3. Decay gamma's: The Darmstadt gamma ray atlas [4]has been built into the ORIHET code. The spectrum after a 1 year irradiation at 1.5 mA is used and is shown in Fig. 6. The source strength is $2.9 \cdot 10^{16}$ photons/sec and 3.2 kW. The source is assumed uniformly distributed in a 1 m long target.

The source strength distributed throughout the target is $4 \cdot 10^{16}$ photons/sec and 17.5 kW. The calculated escape spectra after transport through the target are shown in Figs. 4, 5 and 6, with

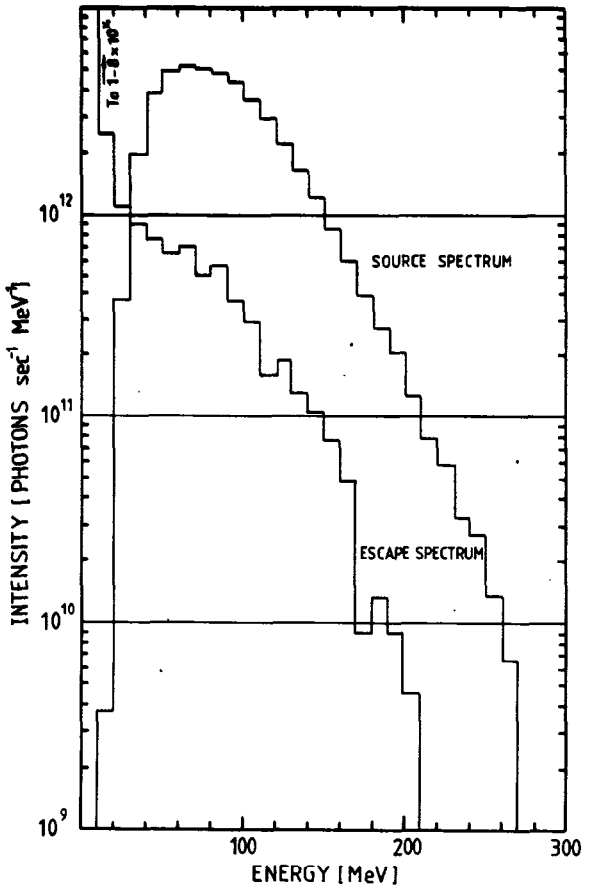

Fig. 5
Integrated source and surface-escape spectra for gammas from π^o decay

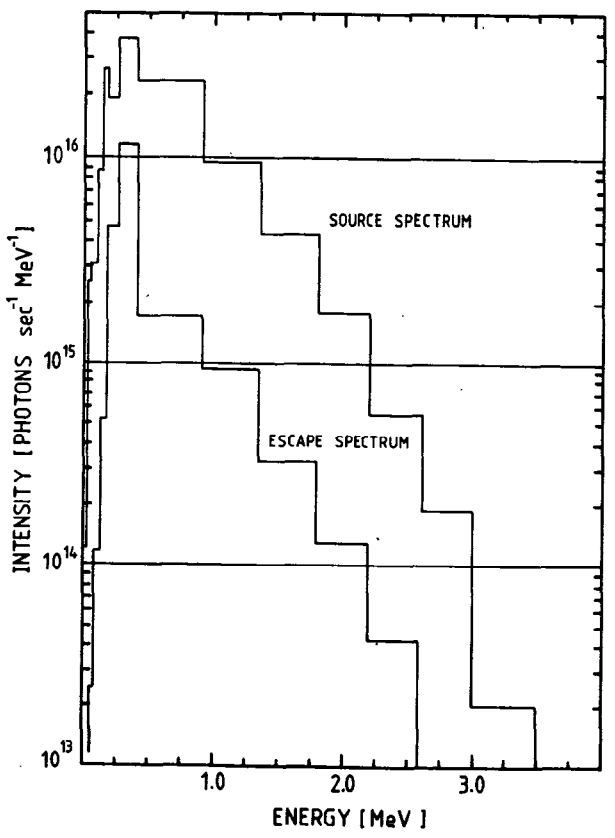

Fig. 6
Integrated source and surface-escape spectra for decay gammas

their source spectra. The overall escapes correspond to $8.5 \cdot 10^{15}$/sec and 3.9 kW, which is approximately 20 % of the source strength.

There are also $9.4 \cdot 10^{13}$/sec of electrons and positrons with mean energy 23 MeV (0.34 kW) escaping the target.

The distributions of escape-gamma intensity and power along the target are shown in Fig. 7. The localized π^0 and nuclear gamma ray production leads to the asymmetric distribution.

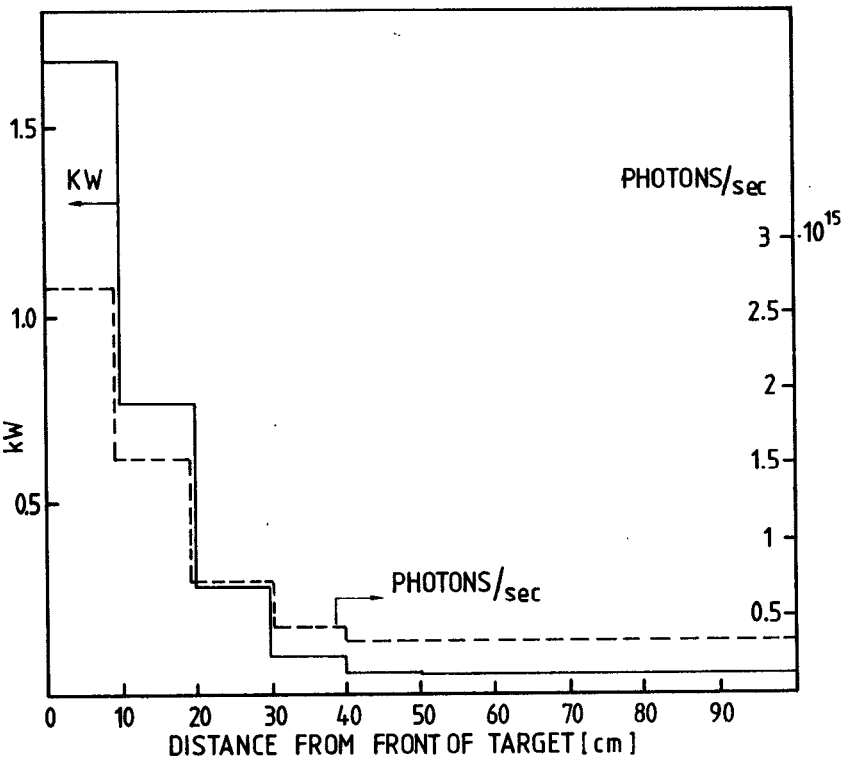

Fig. 7
Calculated distribution of surface-escape gamma flux and power for a 5 cm radius Pb/Bi target

3. THE MODERATOR

The outline design incorporates a 1 to 1.5 m radius D_2O tank of height 2 to 2.5 m. A cold source viewed by beam guides is to be incorporated. Tangential thermal neutron tubes and thermal neutron guides are also planned. The design study has as main aims, to find an optimum moderator volume and the best positions for:

(a) the thermal beam tubes, subject to obtaining an adequately low background;

(b) the cold source, taking into consideration a realistic thermal load on the refrigerator system.

3.1 Thermal Fluxes

Measurements of thermal neutron fluxes in a realistic model of our neutron source have been carried out as part of the SIN/KFA-Jülich collaboration. Some of these measurements have already been reported [5].

The following configurations are of particular interest, both from the point of view of thermal neutron flux maximization and also for consideration of the target/moderator interface design. A general layout of the measured system is shown in Fig. 8; further details of the experiment may be found in reference [5].

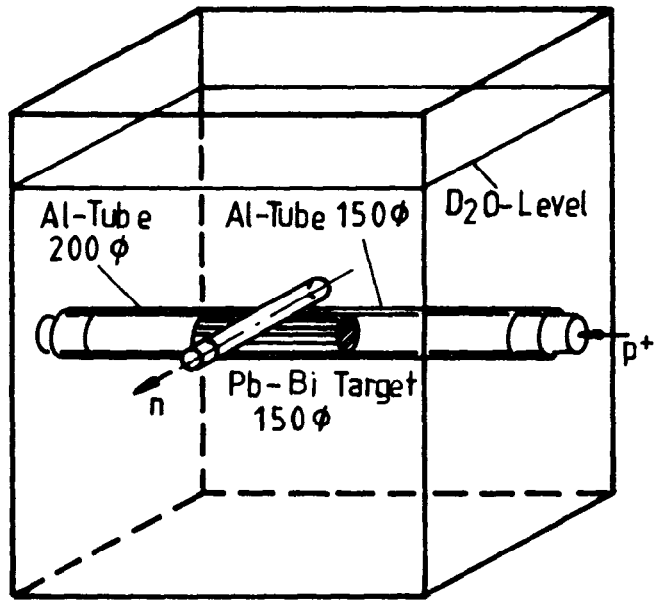

Fig. 8
General arrangement for thermal neutron flux measurements

The results from four configurations are considered:

A) Pb/Bi target + D_2O moderator
B) Pb/Bi target + 3 cm air gap (void) + D_2O moderator
C) Pb/Bi target + 5 cm Be + D_2O moderator
D) Dep.U target + 5 cm Be + D_2O moderator

For the purpose of discussion, A) is taken as a reference system. The thermal flux as a function of radius for two axial distances along the target is shown in Fig. 9 for systems A), B) and C): For further comparison, the flux-maps for cases A) and C) are shown in Fig. 10.

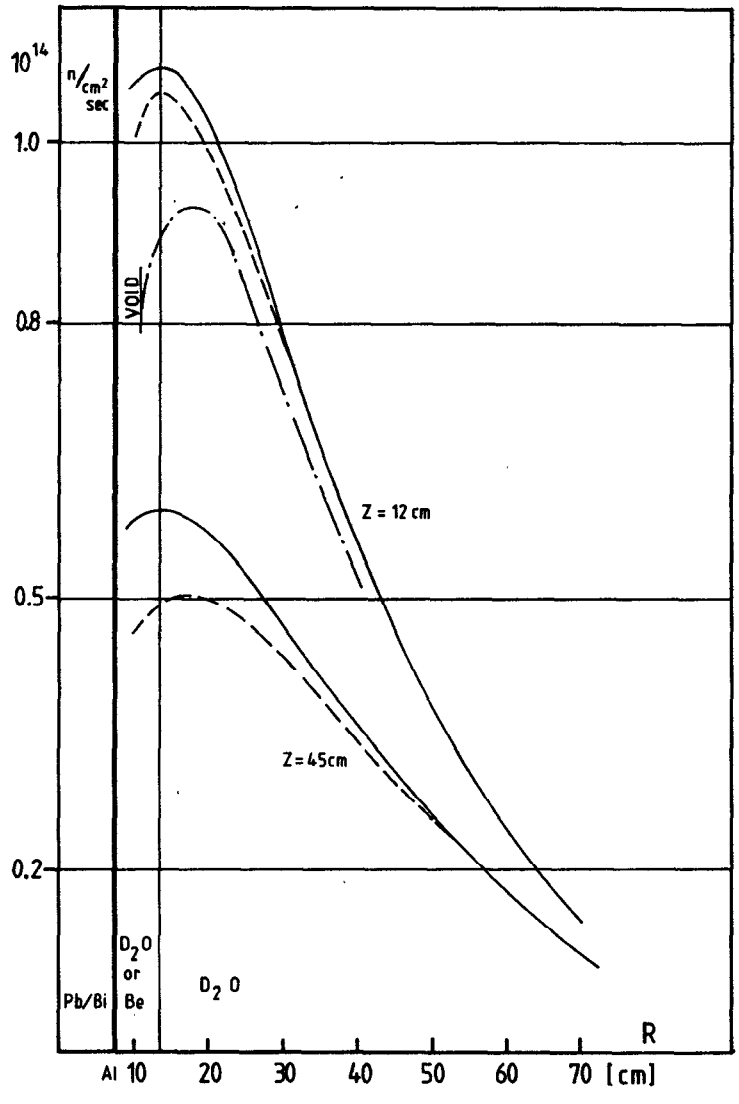

Fig. 9
Measured variation of thermal neutron flux in a D_2O moderator as a function of radial distance from the target axis. Z is measured from the front surface of the target.
(———) case A)
(-·-·-·-) case B)
(------) case C)

The 3 cm void of case B) leads to a peak thermal flux depression of 15 %, with an outward shift of approximately 5 cm. At larger radii, the flux penalty is of the order of 8 %. The effect of the void is to create an additional leakage path for neutrons.

Case C) has produced the most surprising result; although the peak thermal neutron flux is reduced by approximately 2 %, at large radii the fluxes are identical. There seems to be no overall neutron gain with a Be sleeve. In the axial direction the flux decrease with the Be sleeve is somewhat faster, as may be seen in Fig. 10. The gain factor, as estimated from the measured spectra of Cierjacks et al. [6] and published Be(n,2n) cross-section values [7], was approximately 14 %. The measurements indicate the increased absorption by the Be should reduce this

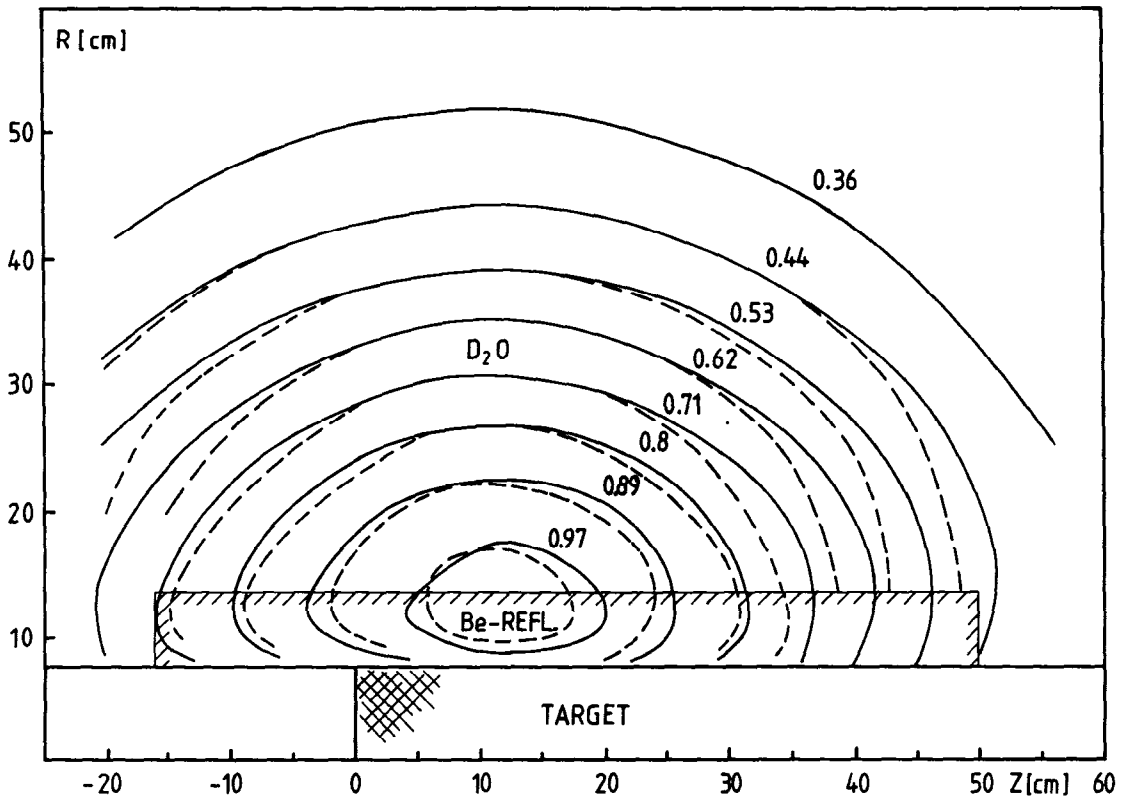

Fig. 10
Measured thermal-neutron flux map in a D_2O moderator. The curves are marked with intensity as a fraction of peak flux.
(———) case A)
(------) case B)

gain factor to about 9 %. This is a significant over-estimate; of the several possibilities, we believe the most probable cause to be, that the neutron spectrum used in the calculation is too hard. Further examination of this question is in progress.

These experimental measurements give us valuable results for code verification. Both diffusion theory and Monte-Carlo [8] give reasonable agreement with experiment. The discrepancy noted in reference [8]may arise from an overestimate for the absorption in the target; this is currently under investigation.

Further indications from these results are:

(i) Any void (for example a vacuum jacket) around the target should be kept to the smallest practicable width.
(ii) Beryllium could be a candidate for a target container material.

Case D) has been included to give an evaluation of depleted uranium as a target material. The thermal neutron flux at the peak was increased by 70 %, which should be compared to the source strength gain of 2.8 compared to Pb/Bi as measured by Bauer et al. [5]. The flux depression of 40 % is caused by the absorption of neutrons in the uranium. The peak flux position is shifted outwards by approximately 4 cm, a definite advantage for installation of beam tubes.

The model target, being solid, was highly unrealistic, lacking for instance any cooling medium and cladding. The considerable uranium density decrease in a technologically feasible target will lead to a further reduction of flux, which has been estimated to be at least 20 %.

The flux increase using depleted uranium would not seem to justify overcoming the prodigious technological problems its use would require.

3.2 Moderator Optimisation. I - D_2O Shield Interface

The moderator flux in the D_2O is affected by (among other things) the choice of material outside the tank. In contrast to the simplest system where the shielding iron starts immediately after the D_2O tank, a layer of material of one of the following two classes could be included:

(i) Combining good reflection and shielding properties, e.g. Pb, Bi.
(ii) Thin layer reflectors, e.g. H_2O, Be.

In both cases a reduction of both the radius of the D_2O tank and the outer shield are possible. An analytic method is used.

Case 1: A Pb reflector

To calculate the optimum thickness for the layer, the overall shielding effect of Pb plus iron is maximized subject to a constant thermal neutron flux in the moderator. Referring to Fig. 11, the thermal flux will be unchanged if $\hat{R}$ (=[R_{D_2O} + ℓ], R_{D_2O} the D_2O tank radius) is kept constant. The extrapolation length ℓ.

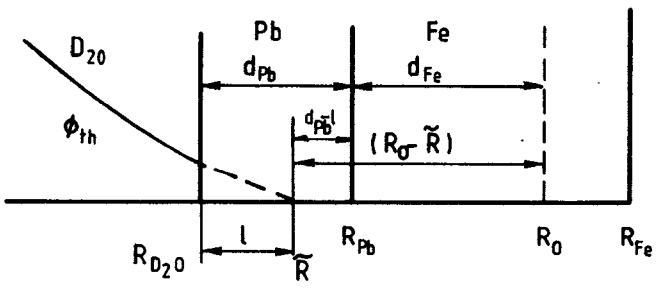

Fig. 11
Explanation of the symbols for calculation, of optimum Pb reflector thickness.

is a function of the thickness of the Pb layer, d_{Pb}, and will be longer for Pb than Fe. The marginally inferior shielding ability of Pb will be offset by it, in part, replacing some of the outer layer of D_2O.

The dose from the high energy neutrons at some radius R_o within the Fe shield may be considered in terms of a shielding function f, given by:

$$f = \text{EXP } -[\Sigma_{Pb} d_{Pb} + \Sigma_{Fe} d_{Fe}]$$

where Σ_{Pb} (= 0.058/cm) and Σ_{Fe} (= 0.062/cm) are the macroscopic shielding cross-sections. Using the dimensional relationships shown in Fig. 11 the function f may be rewritten as:

$$f = \text{EXP } -[\Sigma_{Fe}(R_o - \tilde{R})] \cdot \text{EXP } -[\Sigma_{Pb} d_{Pb} - \Sigma_{Fe}(d_{Pb} - \ell)]$$

$$= \text{EXP } -[\Sigma_{Fe}(R_o - \tilde{R})] . f^*$$

As $(R_o - \tilde{R})$ is a constant, the minimum high energy flux may be found from the condition,

$$\frac{df^*}{d(d_{Pb})} = 0$$

The relationship between ℓ and d_{Pb} may be represented by the Albedo formula for thermal neutrons in the diffusion approximation:

$$\ell = \frac{D_{D2O}}{D_{Pb} \cdot X_{Pb}} \text{ TANH } [X_{Pb}(d_{Pb} + \ell_{Pb})] \qquad (1)$$

where D_{D2O} (= 0.818 cm) and D_{Pb} (= 0.907 cm) are the diffusion coefficients, $X_{Pb} = \sqrt{\Sigma_{abs}/D_{Pb}}$, Σ_{abs} (= 0.00483 cm) is the macroscopic absorption cross-section for Pb and ℓ_{Pb} (= 3.58 cm) is the diffusion theory extrapolation length for a Pb/Fe interface.

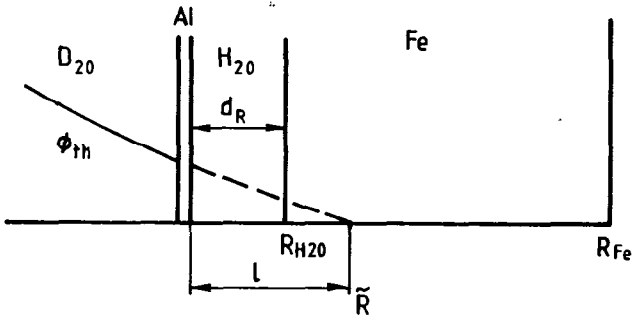

Fig. 12
Explanation of the symbols for calculation, of optimum H_2O reflector layer thickness.

The optimum Pb layer thickness is 23.45 cm and the corresponding extrapolation length 11.88 cm. The diffusion theory extrapolation length for a D_2O/Fe interface is 3.22 cm, hence for $\tilde{R}$ constant and constant flux in the moderator, 8.66 cm of the Pb layer replaces D_2O. The other 14.79 cm of Pb replaces Fe, but as the Pb layer is equivalent to $(\Sigma_{Pb}/\Sigma_{Fe})^*$ 23.45 = 21.88 cm of Fe, then the effective thickness of the shield is increased by 7.09 cm of Fe, which may be removed. (We note that the distance factor in the shielding allows us to take only a large fraction of these 7.09 cm.)

Case 2: A H_2O layer

In this case there is no strong shielding effect to consider, and the problem is to find the H_2O width, d_R, which minimised the iron shield radius R_{Fe} (see Fig. 12) that is:

$$\frac{d(\ell - d_R)}{d(d_R)} = 0$$

The extrapolation length ℓ is related by equation (1) on the previous page, with the appropriate changes due to the different materials and leads to optimum d_R and ℓ given by:

$$D_R = \frac{1}{\chi_{H_2O}} \text{ ACOSH } \sqrt{\frac{D_{D_2O}}{D_{H_2O}}} - \ell_R$$

$$\ell = \frac{1}{\chi_{H_2O}} \sqrt{\frac{D_{D_2O}}{D_{H_2O}} \left(\frac{D_{D_2O}}{D_{H_2O}} - 1\right)}$$

Taking ℓ_R for the H_2O/Fe interface = 0.6 cm, D_{H_2O} = 0.1532 cm and Σ_{abs} for H_2O as 0.0188 cm, then d_R = 3.62 cm and ℓ = 13.72.

The D_2O tank radius may be reduced by 10.5 cm and the outer shield radius is reduced by 6.88 cm.

The reduction of shielding and D_2O material quantities in the case of H_2O and Pb reflectors are comparable. For the D_2O, a 10 cm reduction of tank radius is significant, whilst the shielding thickness change in the case of Pb is small compared to the error involved in estimating the required thickness. It is likely that the innermost layers of shielding will require cooling; a light water cooling channel of about 3.6 cm width would be a neutronic optimum.

3.3 Moderator optimization. II - Physical dimensions

The size of the D_2O moderator affects the thermal neutron flux. Two different criteria apply:

(i) for beam tubes the maximum neutron current at the monochromator;
(ii) for guides and the cold source, the maximum flux of the moderator.

In this section, the optimisation for beam tubes is considered. The neutron current, I, at a monochromator is determined by the flux at the beam tube tip, ϕ, and the length from tip to monochromator L. The length L is determined principally by the radius of D_2O tank and the thickness of the bulk shield; reduction of L can only come from reduction of the D_2O tank radius for a properly shielded source.

Taking as a reference system, a 145 cm long by 15 cm diameter target in a 130 cm radius by 260 cm high D_2O tank (see Fig. 13), the thermal neutron flux distributions in the moderator, with three thicknesses of the whole peripheral layer of D_2O replaced by Pb, have been calculated using the DIFF-2D code of RSYST. Calculated axial and radial flux distributions are shown in Figs. 14 and 15.

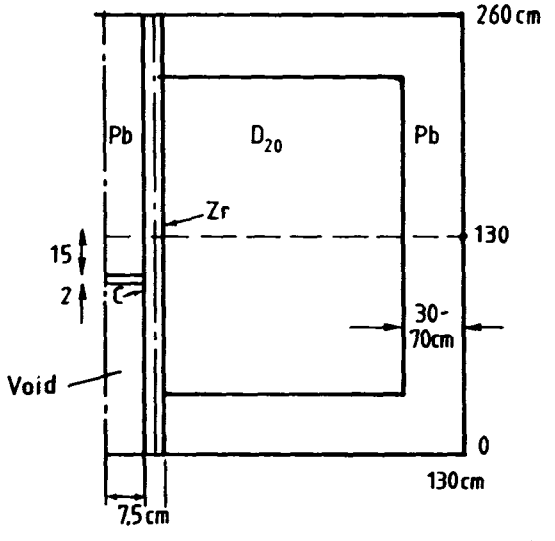

Fig. 13
Arrangement of target/ moderator/reflector assembly for calculation of optimum D_2O tank radius in section 3.3.

The figure of merit η for examining the performance is:

$$\eta = \frac{I}{I_{Ref}} = \frac{\phi}{\phi_{Ref}} \left(\frac{L_{Ref}}{L}\right)^2$$

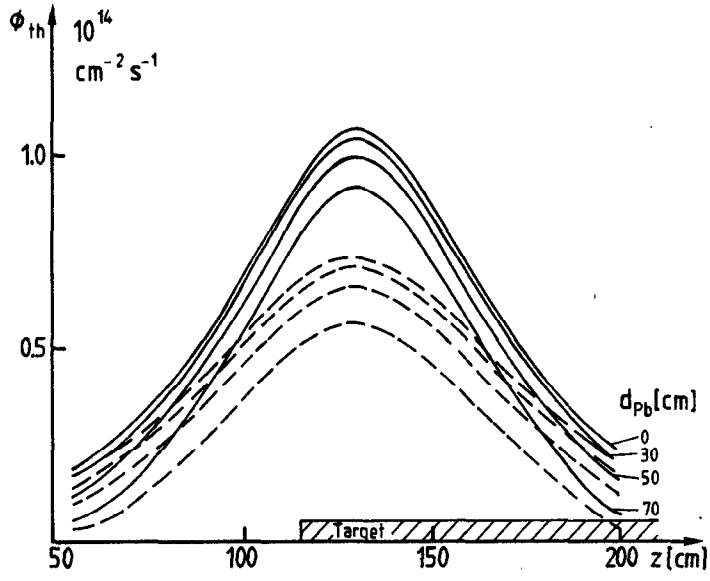

Fig. 14
Variation of neutron flux at radial distances of 16.25 cm (———) and 36.25 cm (------), from the target axis in the target axial direction. Calculation by diffusion theory for 0, 30, 50 and 70 cm of D_2O replaced by Pb.

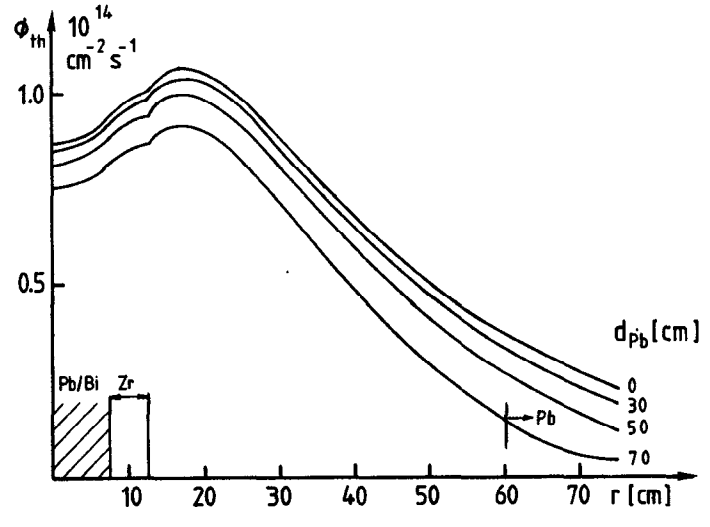

Fig. 15
Radial distribution of neutron flux in plane of the flux maximum from diffusion theory calculation. Curves are for 0, 30, 50 and 70 cm of D_2O replaced by Pb.

In Table II are shown values of η and ϕ for the reference system and three other 'effective' D_2O tank radii, at three different radii, r, in the D_2O. Taking r = 31.25 as a representative case, an effective D_2O tank radius of approximately 100 cm seems optimal. Using the extrapolation length for the H_2O layer of the previous section, this corresponds to a physical radius of approximately 90 cm.

Table II

Fluxes and figure of merit η for various D_2O tank effective radii

$\tilde{R}$(cm)	L(cm)	r = 16.25 cm		r = 31.25 cm		r = 42.5 cm	
		$\phi\ 10^{14}$ cm^{-2} sec^{-1}	η	ϕ	η	ϕ	η
131.6	600.0	1.027	1.0	0.826	1.0	0.606	1.0
112.0	580.4	1.002	1.043	0.798	1.032	0.575	1.014
92.3	560.6	0.959	1.070	0.748	1.036	0.520	0.984
72.3	540.7	0.881	1.057	0.655	0.977	0.419	0.851

3.4 Energy Deposition

The energy deposition by the fast neutrons during thermalisation has been calculated, but at present only an upper bound estimate for the other contributions is available. The following contributions to the total energy have been calculated for a 1 mA current:

1. High energy neutrons	42.0	kW (UL)
2. High energy protons	0.8	kW (UL)
3. Charged pions	0.14	kW (UL)
4. During thermalisation	18.2	kW (C)
5. Gammas (from target)	2.6	kW (UL)
6. Electrons (from target)	0.23	kW (UL)
7. Gammas (from D[n,γ]T)	2.7	kW (C)

where the qualifiers UL stand for Upper Limit and C for Calculated.

This gives an upper limit of approximately 67 kW/mA.

The distribution of energy deposition by the neutrons during thermalisation indicates that 50 % of their power contribution is deposited in approximately the first 6 cm of the D_2O and 90 % in the first 22 cm. The peak energy density for this contribution is 1.0 W/cc at 1 mA.

3.5 Moderator Activation

The tritium build-up has been estimated from the thermal flux distribution in the D_2O, using a macroscopic capture cross-section of 0.000034/cm. Averaging over the flux, the capture rate is estimated at $2.7 \cdot 10^{15}$/sec/mA. This corresponds to an equilibrium

activation of approximately 70 kCi. For a total D_2O volume of 4850 litres, this is an equilibrium specific activity, with mixing, of 14.4 Ci/ℓ.

The values during the build-up are 0.8 Ci/ℓ at 1 year, 1.5 Ci/ℓ at 2 years and 2.3 Ci/ℓ at 3 years.

REFERENCES

[1] W.E. Fischer, Status Report on the SIN Neutron Source, These proceedings
[2] Y. Takeda, Thermofluid Dynamics of the Liquid Lead-Bismuth Target for the Spallation Neutron Source at SIN, These proceedings
[3] W. Litzow et al., Paper 4, SNQ-Report, part III, A2 (1981)
[4] U. Reus, W. Westmeier, I. Warneche, GSI-Report 79-2 (1979)
[5] G. Bauer et al., Contribution ICANS V (Jülich) p. 445 (1981)
[6] S. Cierjacks et al., Contribution ICANS IV (Tsukuba (1980)
[7] Много групповые методы расчета защиты от неитронов Б.Р. Бергельсон, А.П. Суворов, Б.З.Торлин (1970)
[8] F. Atchison et al., SIN Newsletter 14, p.NL5 (1982)